Bioconjugated solid lipid nanoparticles (SLNs) for targeted prostate cancer therapy

Mushfiq Akanda[a], Giullia Getti[a], Uttom Nandi[a], Md Sadeque Mithu[a], Dennis Douroumis[a,b1]

[a] Medway School of Science, Faculty of Engineering and Science, University of Greenwich, Chatham Maritime ME4 4TB, Kent, United Kingdom

[b] Centre for Innovation & Process Engineering Research, Chatham Maritime, ME4 4TB, Kent, United Kingdom

[1] CIPER Centre for Innovation and Process Engineering Research, Kent, ME4 4TB, UK,
Email: d.douroumis@gre.ac.uk

Abstract

Prostate cancer is one of the prominent causes of cancer mortality in men all over the world and a challenge to treat. In this study, transferrin (Tf) bioconjugated solid lipid nanoparticles (SLNs) were developed and loaded with curcumin (CRC) for active targeting of prostate cancer cells. Curcumin is an anticancer agent, but its clinical applications are impeded due to the poor water solubility and bioavailability. Prepared blank Tf-SLNs showed minimal cytotoxicity while Tf-CRC-SLNs demonstrated significant *in-vitro* anti-proliferative activity compared to CRC-SLNs alone. Cellular uptake of Tf-CRC-SLNs were found to be significantly higher ($p<0.05/=0.01$) compared to unconjugated SLNs or pure drug alone. Bioconjugated Tf-CRC-SLNs also showed improved early apoptotic and late apoptotic or early necrotic populations (6.4% and 88.9% respectively) to CRC-SLNs and CRC solution. Most importantly, *in-vivo* studies with Tf-CRC-SLNs in mice bearing prostate cancer revealed significant tumour regression (392.64 mm^3 after 4 weeks, $p<0.001$) compared to the control group. The findings of this work encourage future investigations and further *in-vivo* clinical studies on the potential of bioconjugated SLNs for cancer cure.

Keywords

Solid lipid nanoparticles; curcumin; transferrin; prostate cancer; bioconjugation.

1. Introduction

Among many type of malignancies, prostate cancer is one of the leading cause of cancer mortality in middle age male population around the world [1-3]. The prostate cancer development inside the human body is known to be a multistage process which starts with a small latent carcinoma and progress towards high grade metastatic cancer overtime. Advanced techniques have been introduced to diagnose and categorize stage or grade of the tumour growth using digital rectal imaging, serum prostate specific antigen measurement and transrectal ultrasound [4]. Accordingly targeted therapeutic approaches have been introduced to treat prostate cancer such as folate-conjugates liposomes and polymer-peptide-enveloped drug-loaded copper sulphide nanoparticles [5,6]. Patil *et al.*, prepared folate – targeted liposomes loaded with a mitomycin C prodrug and doxurobicinfor PSMA positive cancer cells [5]. Those nanoparticles presented increased cell drug levels compared to non–targeted liposomes when incubated with LNCaP cells. Another novel approach introduced by Poudel *et al*., involved encapsulated docetaxel in copper sulphide nanostructures functionalized by a polymer peptide [7]. The conjugated nanoparticles were effectively endocytosed by somatostatin receptors while presented better loading efficiency and NIR responsive release for the anticancer agent. Furthermore, the developed nanoplatform demonstrated improved accumulation, tumour ablative behaviour, low cytotoxicity and biocompatibility.

In order to achieve prostate-specific drug delivery of a folate-targeted amphiphilic cyclodextrin was developed using fusogenic DSPE-PEG_{5000}-folate [8]. Endosomal release of siRNA was achieved through 200 nm nanoparticles with neutral surface charge. These complexes protected siRNA from serum nucleases but when excess amount was incubated with free folate the uptake in LNCaP was decreased. Kaushik *et al*. developed solid lipid nanoparticles using a range of lipids such as palmitic acid, stearic acid, cetyl palmitate and glyceryl monostearate for the delivery of docetaxel in MCF-7 breast cancer cells [9]. Among these, the stearic acid SLNs showed high apoptotic index compared to free drug, enhanced solubility but also presented lower plasma protein binding and far better pharmacokinetic and pharmacodynamic profiles in animal studies. Other examples of similar nanoparticulate drug delivery systems include proteins and polypeptides, cyclodextrins, gold nanoparticles, Zein

nanoparticles , folate targeted cyclodextrin (CD) nanoparticle, and self-assembling poly(ethylene glycol)-block-polylactide conjugate nanoparticles [10–15].

Solid lipid nanoparticles (SLNs) are considered as a novel colloidal drug delivery system (DDS) that successfully combines the qualities of liposome and polymeric nanoparticles. SLNs have the ability to provide both stability of the solid core and also biocompatibility of lipid nanocarriers avoiding the limitations related to liposomes and polymeric nanoparticles such as long-term stability, toxicity, sterilization and scale-up [16]. SLNs have been found to increase water solubility, bioavailability and therapeutic efficacy of water insoluble drugs [15–17]. However, similarly to other DDS they are prone to non-specific uptake which limits their efficiency for the prostate cancer treatment. For this purpose, surface modification of SLN has been exploited in order to avoid absorption *via* RES and enhanced tumour selectivity [18 -19].

Kuang *et al*., engineered cRGD-conjugated SLNs and encapsulated a hydrophobic IR-780 dye that could be used as imaging-guided photothermal therapeutic agent with laser irradiation [21]. The SLNs were targeted to cell lines over expressing $a_v\beta_3$ integrin and the results demonstrated tumour eradication. More recently, Karim *et al.* (2018), conjugated a fluorescent-labelled NFL-TBS on lipid nanocapsules to enhance internalisation into human glioblastoma cells [22]. The results showed that increase amounts of bioconjugated peptides enhanced internalization under *in-vitro* conditions. On the other hand, transferrin has been extensively investigated through Tf-mediated drug and gene delivery systems. Overexpression of these Tf receptors in malignant tissues compared to normal tissues is well known due to the higher iron need of malignant cells for rapid growth and division [23]. Due to their high specificity, various Tf conjugated nanoparticles such as PLGA, PEGylated liposomes, gold nanoparticle/ or albumin nanoparticle have been developed for diagnostic and therapeutic purposes [23–26].

In this study, transferrin conjugated SLNs were developed for active targeting of prostate cancer cells. The main objective of this study was to demonstrate the clinical efficacy of the bioconjugated Tf – SLNs using CRC as a model drug. CRC loaded SLNs were optimized using high pressure homogenizer and subsequently conjugated with Tf. The stable nano–dispersions were characterized for particle size distribution, zeta potential and drug loading capacity. Further investigations include cytotoxicity studies, cellular uptake, apoptosis and *in vivo* animal trials. As drug loaded Tf -SLNs have not

fully investigated particularly for the treatment of prostate cancer, the present study explores efficiency of various SLNs as drug delivery system to the tumour site using both *in vitro* and *in vivo* model.

2. Materials & methods

2.1. Materials

Curcumin (CRC), transferrin (Tf), stearic acid (SA), was purchased from Sigma-Aldrich. Poloxamer 188 (P188) was kindly donated by BASF (Ludwigshafen, Germany). 1-ethyl-3-[3-dimethylaminopropy] carbodiimide hydrochloride (EDC) was purchased from Sigma-Aldrich. Bradford assay reagent was purchased from Bio-Rad. All other chemicals and solvents were of analytical and high-performance liquid chromatography (HPLC) grade. LNCaP cell line was purchased from American Type Culture Collection (ATTC: Manassa, Virginia, USA). Dulbecco‘s modified Eagle‘s medium (DMEM), thiazolyl blue tetrazolium bromide (MTT), L-glutamin, Penicillin streptomycin and heat inactivated fetal bovine serum (FBS) and trypsin were all purchased from Sigma -Aldrich (UK). PE Annexin V Apoptosis Detection Kit I from BD Biosciences.

2.2. Methods

2.2.1. SLN’s preparation method

The high pressure homogenisation technique was used to prepare SLN’s for this study. Firstly, stearic acid, the lipid phase was emulsified in the water phase using a high speed homogeniser (T 25 digital ULTRA-TURRAX®, Oxford, UK)). Then a high-pressure homogeniser (Micro DeBee, South Easton, USA) was used for the further processing of the pre-emulsion. In brief, SA (500 mg) and P188 (250 mg) were heated to achieve a melt of these compounds. Then for CRC loaded SLN’s, 50 mg of drug was dissolved in 3 mL ethanol and then incorporated in the molten lipid. The drug comprising molten lipid was dispersed in a hot aqueous phase and homogenised using an Ultra-Turrax T25 (IKA®- WERKE GMBH, Staufen, Germany) homogeniser to form a pre-emulsion. The mixture was then transferred and homogenised in a Micro DeBee (South Easton, MA, USA) high pressure homogeniser and processed at 15,000 PSI for 7 minutes (min) at 70 °C. Then the hot nano-dispersions were left at room temperature (25±1 °C), to crystallise and form lipid nanoparticles with a solid matrix.

2.2.2. Bio-conjugation of transferrin

Transferrin was coupled on the surface of the SLNs by using 1-ethyl-3-carbodiimide (EDC), as described before by Greg *et al*., (1996). Firstly, 10 mg/mL of transferrin was dissolved in PBS (pH 7.2) and then added to the lipid mixture. Afterwards 10 mg/mL EDC was added to the total mixture and agitated using a vortex agitator. The mixture was then left for reaction for 2 h at room temperature. At the end of the reaction, excess EDC and transferrin was excluded from the transferrin conjugated SLN suspension by size exclusion technique using Sepharose CL-4B column. Transferrin (Tf) conjugation efficiency was analysed using Bradford assay.

2.2.3. Methodology of Transferrin assay quantification

Conjugation efficiency of transferrin-SLNs was quantified by Bradford assay where protein concentrations is related to the absorbance change due to binding of Coomassie Blue G-250 and protein molecules. The calorimetric assay appears darker with the increment of protein concentration. The protein concentration in a sample (*e.g.*, Tf-conjugated SLN) is determined in comparison to standard BSA concentrations. Bovine Serum Albumin (BSA) with a concentration range of 0, 0.125, 0.5, 1.0 and 2.0 mg was used to prepare calibration curve. For the analysis, 100 µL of each standard was pipetted in glass tube and 5 mL of the Bradford reagent was added. The mixture was lightly agitated and allowed to stand at room temperature for 5 min before reading at 595 nm using a UV spectrophotometer. For blank, 100 µL of deionised water was pipetted and 5 mL of Bradford reagent was added followed by vortex and UV reading. For TF-conjugated SLN, 100 µL of SLN sample was pipetted and the same procedure as the BSA standard was followed. All tests were carried out in triplicate and a linear regression calibration curve was obtained for BSA standards. The conjugation efficiency was then determined by comparing the absorbance value of the sample solution to the calibration curve.

2.2.4. Particle size and zeta potential study

The particle size and zeta potential of the sample preparations were analysed using dynamic light scattering photon correlation spectroscopy (Malvern Zetasizer Nano-ZS, Malvern, UK). Firstly, sample dispersions were adequately diluted to 0.1 mg/mL with de-ionised water and then particle size was measured in triplicate. After that sample

were transferred into a zeta-cuvette and the net charge present on the particle were again evaluated in triplicates. The z-average and PDI values were applied for the evaluation of the particle size.

2.2.5. Atomic Force Microscopy (AFM)

AFM analysis was conducted using freshly prepared SLN formulations; approximately 3 µL was deposited on the freshly cleaved mica surface (G250-2 mica sheets 1" x 1" x 0.006"; Agar Scientific Ltd, Essex, UK), and allowed to dry for 1 hour (h) at room temperature prior to AFM analysis. Then the images were obtained by scanning the mica surface under ambient conditions using a PeakForce QNM Scanning Probe Microscope (Digital Instruments, Santa Barbara, CA, USA; Bruker Nanoscope analysis software Version 1.40). AFM scanning was done using ScanAsyst-air probes, with tip radius of 2 nm and spring constant of 0.67 N/m; nominal 0.4 N/m). The images were collected from two different formulations by random spot surface sampling at five different areas.

2.2.6. Determination of encapsulation efficiency

Encapsulation efficiency of CRC in the nanoparticles was determined spectrophotometrically at λ_{max} of 425 nm. A calibration curve was established by using UV-vis spectrophotometer and the calibration curve showed good linearity (with R^2 value of 0.991) of concentrations ranging from 1-20 µg/mL. The process was adopted from the worked done by Douroumis *et al.* (2011) [28]. In brief, 1 mL of SLN nanosuspension was centrifuged for 30 min at 40,000 rpm and 25 °C. Then the supernatant from the tube was decanted and the sediment was lyophilized and subsequently dissolved in acetonitrile (ACN). The absorbance of the ACN solution was measured after appropriate dilutions where amount of drug gave a direct measurement of the entrapped CRC amount in SLNs. The following Equations (1) and (2) were used to calculate drug loading and encapsulation efficiency, respectively.

$$\text{Drug loading} = \frac{Amount\ of\ curcumin\ in\ SLNs}{Amount\ of\ SLNs}\ x\ 100 \quad (1)$$

$$\text{Entrapment efficiency} = \frac{Drug\ loading}{Theoretical\ drug\ loading}\ x\ 100 \quad (2)$$

2.2.7. Cell viability test

LNCaP prostate cancer cell lines obtained from American Type Culture Collection (ATTC: Manassa, Virginia, USA) were cultured in DMEM (Sigma, UK) supplemented with 10% v/v foetal bovine serum (SIGMA, UK), 1% L-glutamine/penicillin/streptomycin at 37 ºC and 5% CO_2. The cytotoxicity bulk curcumin in ethanol (10 mg/mL) and drug loaded SLN formulation was examined using MTT (3-(4, 5-dimethylthiazolyl-2)-2, 5-diphenyltetrazolium bromide) assay as previously described [29]. At first, 1 x 10^6 cells/well were seeded in a 24 well flat-bottom plate and incubated for 24 h. Then pure drug and drug loaded SLN formulations were added to the wells at various concentration and again incubated for 24 h. After these treatments, 100 µL of MTT solution (5 mg/mL) was incorporated into each well plate and incubated for another 2 h. The culture medium was replaced with 200 µL of acidified isopropanol to dissolve the MTT formazan crystals and absorbance was collected at 492 nm using a microplate reader (Thermo Scientific Multiskan FC Microplate Photometer). Non-treated cells as well as 2% ethanol treated cells and CRC (10, 20, 40, 50 and 100 µg/mL concentrations) was used as a control for this study. Blank and drug loaded (50 mg equivalent) SLN formulations were incubated at concentrations of 0.18, 0.37, 0.73, 1.11, 1.47 mg/mL to investigate the amount of viable cells.

2.2.8. Cellular uptake analysis by fluorescent microscopy

A Nikon fluorescent microscope (USA) was used to study the uptake of drug loaded SLN formulations. The study was done using a 24 well flat bottom plate where 20 X 10^3 cells were seeded on a round shaped cover slip in each well and incubated for 48 hours. Then various concentrations of drug loaded SLN formulations were added into each well and incubated with the cells for 24 h. After the incubation, the media was discarded, and cells were washed using 2 mL of PBS. Finally, 1 mL of 4% paraformaldehyde was added to the each well to fix the cells on the cover slips and left in the dark for 15 min. The paraformaldehyde was discarded from the well and cells were again washed three times with 1 mL PBS and mounted on a glass slide using VECTA SHIELD mounting medium containing DAPI. Then images were acquired using the Nikon ECLIPSE 90i overhead epifluorescent microscope attached to a Nikon

digital camera (DS-Qi1Nc) and a computer running Nikon NIS-Elements Advanced Research software. The principal objective used for fluorescent imaging was an oil immersion CFI Plan Apochromat VC 60X N2 (NA1•4, WD 0•13 mm).

2.2.9. Cellular uptake analysis by flow cytometry

For the study, 2×10^4 cells/well were seeded on cover slips in a 24 well flat-bottom plate. and treated with pure curcumin and drug loaded SLN formulations (10 µg/mL) for 24 h. After incubation, cells were trypsinized, washed with 1 mL PBS**,** re-suspended in 500 µL of PBS and studied using Accuri C6 flow cytometer (BD, UK). The gated population was set based on the size and granularity of the untreated cells and analysed using a solid-state blue laser with a 488 nm excitation spectrum, a detector of FL1 path with filter 530/30 nm to quantify the percentage of curcumin containing cells. A minimum of 10,000 gated events was acquired to calculate the total population of viable LNCaP cells and data was analysed using the Accuri C6 software.

2.2.10. *In-vitro* apoptosis study

The apoptosis capability of SLNs in LNCaP cells were studied using a PE Annexin V assay kit I from BD Biosciences. Firstly, 1 x 10^6 cells were seeded in each well of a 24 well flat-bottom plate and incubated for 24 h. After that the blank and drug loaded SLN formulations and pure CRC were added to the 24 well plates at a concentration of 25, 50 and 100 µg/mL where untreated cells were used as negative control. After 48 h of incubation, the cells were trypsinized, centrifuged and washed twice with 5 mL of PBS. The pelleted cells were re-suspended in 500 µL of 1x binding buffer, 5 µL PE Annexin V and 5 µL of 7-Amino-Actinomycin (7-AAD) and incubated in dark for 10 min. Samples were analysed on the Accuri C6 flow cytometer for PE and 7AAD expression. Cells were considered early apoptotic when PE positive and 7AAD negative and all experiments were performed in triplicates**.**

2.2.11. Treatment of mice bearing human prostate cancer xenografts

In-vivo studies were undertaken in collaboration with Pasteur Institute, Greece. House and feed purchased female nude mice aged 6-8 weeks under standard conditions kept in a 12 h light/ 24 h dark cycle. LNCaP prostate cancer cell line was cultured in a complete culture medium DMEM. Prostate cancer xenograft was established by

injecting 2 x 10^6 LNCaP cells (in 100 µL of PBS) into the fat pad of mouse mammary glands. Tumour allowed to grow for 3 days without any treatments and monitor the tumour volume daily by measuring two perpendicular tumour diameters with a calliper [tumour volume mm^3] = (length [mm]) x (width [mm])^2 x 0.52. Afterwards the mice with the prostate cancer xenograft were divided into five groups (n=6/group) according to the treatment received: The blank control, CRC solution, Blank SLN, CRC encapsulated SLN (CRC-SLN) and Tf conjugated CRC loaded SLN (Tf-CRC-SLN). For CRC based treatments, 10 mg/kg of CRC was administered. The treatments were administered by injecting intravenously *via* mice tail (two injections per week with injection volume of 200 µL for 4 weeks). Then tumour size measurements and animal weight were taken twice a week.

2.2.12. Statistical analysis of tumour regression

All the data were analysed and presented as a mean along with their standard deviation (n=3). T-test analysis was also carried out to compare statistical significance between blank and drug loaded SLN formulations on LNCaP prostate cancer cell line. Significant variation in the comparison were considered when probability or p-value was found to be less than 0.05.

3. Results and discussion

3.1. Morphology analysis of SLNs

Nanoparticles of both loaded and unloaded SLNs were prepared by using lipid and surfactant crude dispersions under high pressure homogenization processing. HPH is an established technology for the engineering of SLNs whereby controlling the temperature and the applied pressure nanodispersions with uniform particle size can be produced. It was found that SLNs with reproducible sizes could be formed with homogenization temperatures exceeding the melting point of lipid and pressures up to 500 bars.

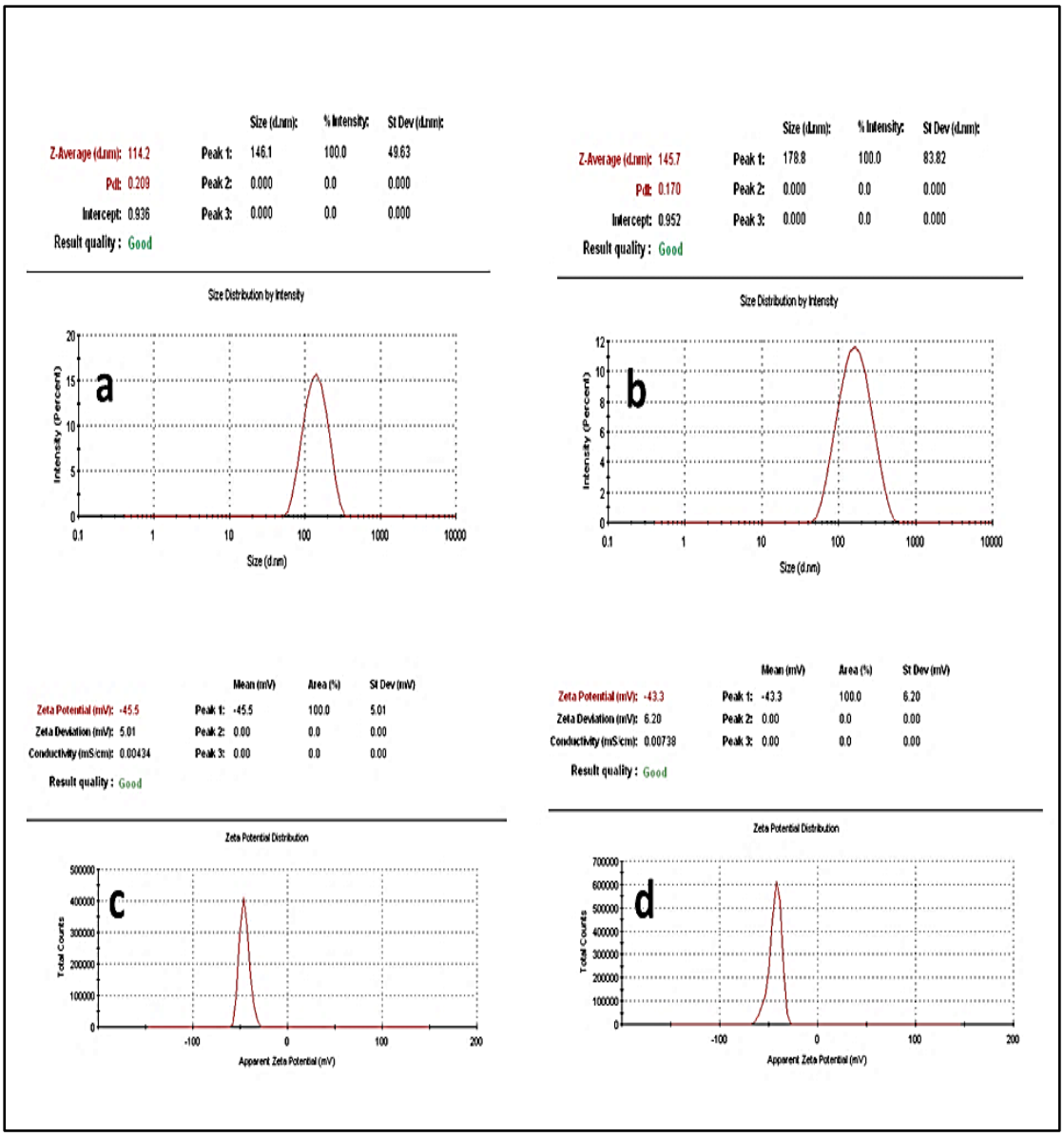

Fig. 1: Particle size distribution of **(a)** BL-SLN, **(b)** BL-Tf-SLN, and zeta potential of **(c)** BL-SLN, **(d)** BL-Tf-SLN (BL- blank)

The physical properties of SLNs measured by size and zeta potential before and after transferrin conjugation are given in Table 1. All SLN dispersions showed very good polydispersity of less than 0.2 suggesting narrow size distribution, which in turn can also be considered as a homogenous distribution [30]. Fig. 1 shows typical SLN narrow particle size and zeta potential for the obtained blank non-conjugated and conjugated nano-dispersions. The mean particle size of blank SLNs before and after the Tf conjugation was 145.1 nm and 153.3 nm respectively. SLNs presented very good stability over a period of six months at 4°C with minor increase in particle size varying from 5–7 nm.

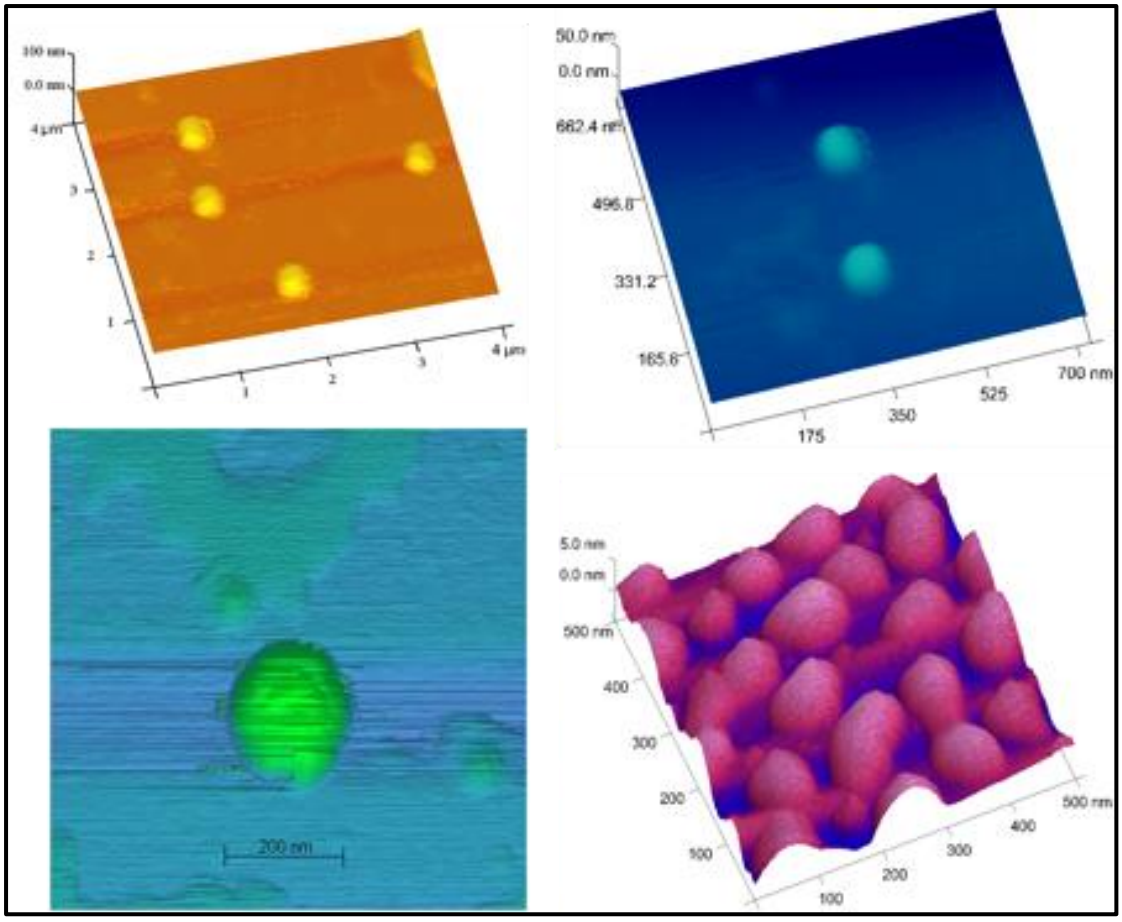

Fig. 2: AFM images of bioconjugated Tf -SLNs loaded with CRC.

As expected, drug loaded SLNs presented a substantial particle size increase due to the CRC encapsulation form 218.5 nm to 231.4 nm for CRC-SLN and Tf-CRC-SLN respectively). The zeta potential of blank SLNs and CRC-SLNs was -18.74 mV, -8.11 mV respectively, while Tf-SLN and Tf-CRC-SLN presented zeta potential at -18.35 mV and -8.36 mV, respectively. However, unconjugated and Tf conjugated SLNs showed little to no change in their surface charge before and after conjugation process. As shown in Table 1, both the particle size distribution and zeta potential of all SLNs demonstrated non-significant ($p>0.05$) increase for a period of 6 months suggesting excellent dispersion stability. However, a decrease in the zeta potential for CRC loaded SLN dispersions (both conjugated and un-conjugated) was observed.

As known from previous studies, SLNs stability is partially related to its packing materials [31]. In this study, CRC was encapsulated inside the solid lipid core which resulted in the reduction of the zeta potential value for CRC-SLN. Although, the decrease of zeta potential is considered as an indication of possible particle aggregation in this particular instance but there was no impact on the dispersion's stability. In fact,

the zeta potential of CRC loaded formulations showed slight increase over a period of six months which is an indication of satisfactory electrochemical and physical stability. Poloxamer P188 is a non-ionic surfactant which is known to adhere onto the nanoparticle by forming a coating around the outer layer [32]. The presence of poloxamer in the nanoparticles has stabilised the dispersion by decreasing electrostatic repulsion [32-34].

Table 1: Measurements of particle size distribution and zeta potential of SLN formulations (n= 3)

	Months	**Particle size (nm)**		**Zeta Potential (mV)**	
		Blank	**CRC Loaded**	**Blank**	**CRC Loaded**
Unconjugated SLN	1	145.1 ±2.7	218.5 ±3.7	-18.74 ±1.6	-8.11 ±0.1
	3	147.8 ±3.5	221.3 ±1.9	-18.38 ±2.4	-7.95 ±0.5
	6	149.1 ±1.1	223.7 ±2.0	-17.95 ±0.31	-7.93±0.3
Tf -SLN	1	153.3 ±0.9	231.4 ±2.5	-18.35 ±1.3	-8.36 ±0.1
	3	155.1 ±3.6	233.1 ±2.6	-18.11 ±1.2	-8.10 ±0.5
	6	158.8 ±3.3	233.6 ±1.4	-18.01 ±0.1	-8.09 ±0.2

It can also be seen from Table 1 the transferrin (Tf) conjugation resulted in particle size increase of approximately 7 nm for blank SLNs. Similarly, the Tf conjugation of CRC loaded SLNs resulted in particle size increase from 218 nm to 231 nm. The particle size increase is related to the size of Tf molecule on the surface of SLN particles. Furthermore, as shown in Fig. 2 AFM analysis revealed nanoparticles with spherical morphology and particle size varying from 200-220 nm. The results are quite similar with those obtained by laser diffraction and small differences were attributed to the absorption of SLNs on the mica substrate.

The conjugation reaction of Tf on SLN surface was similar to the one proposed by Greg, 1996 (Fig. 3) and achieved by using EDC as an activator [34]. EDC is known to activate -COOH groups (SLNs) by creating an active ester intermediate. In the presence of amine nucleophile, (Tf) an amide bond is formed followed by the release of an iso-urea by-product. The amount of the conjugated Tf on SLNs was quantified by Bradford assay, as previous studies suggested [35]. The conjugation efficacy was found to be 7.3 mg/mL (Tf) per 25 mg/mL of lipid suggesting a highly efficient conjugation process [35].

3.2. Determination of encapsulation efficiency (EE) and drug loading (DL)

The encapsulation efficiency of both CRC-SLN and Tf-CRC-SLN was estimated for the evaluation of the effectiveness of the drug-carrier system and the homogenisation process for the nano–encapsulation. The EE for CRC-SLN dispersions was estimated at 91.7% while for Tf-CRC-SLN at 91.1%. Interestingly, the inclusion of Tf did not hamper the encapsulation efficiency of CRC in SLN as it resides as an outer coating on the nanoparticle.

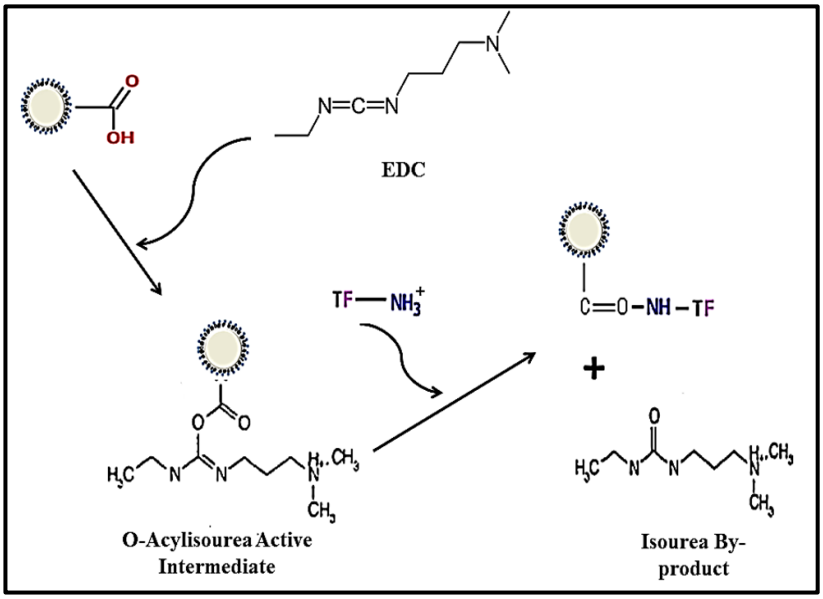

Fig. 3: Mechanism of conjugation (Bioconjugate Techniques by Greg T. Hermanson, Academic Press Inc. 1996)

Table 2: Drug loading and entrapment efficiency of CRC-SLN and Tf-CRC-SLN

Formulation	Drug loading (%)	Encapsulation efficiency (%)
CRC-SLN	6.5	91.7
Tf-CRC-SLN	6.3	91.1

Also, the solubility of CRC in the lipid matrix is a vital factor for drug loading and it has facilitated the encapsulation of CRC inside the lipid matrix [36]. Table 2 depicts the DL and EE values of CRC-SLN and Tf-CRC-SLN. However, the DL values were low for both drug carrier systems. It was observed that the drug loading of higher CRC amounts resulted in unstable dispersions where the drug precipitated out of SLNs in the form of crystals within a few days.

3.3. Antiproliferative effect of CRC and SLN nano-dispersions

The antiproliferative effect of CRC-SLN and Tf-CRC-SLN was compared to an alcoholic solution of CRC and empty SLN formulations in LNCaP cancer cells. As shown in Fig. 4 the cytotoxicity studies of pure curcumin presented strong anti-proliferative activity after 24 h incubation.

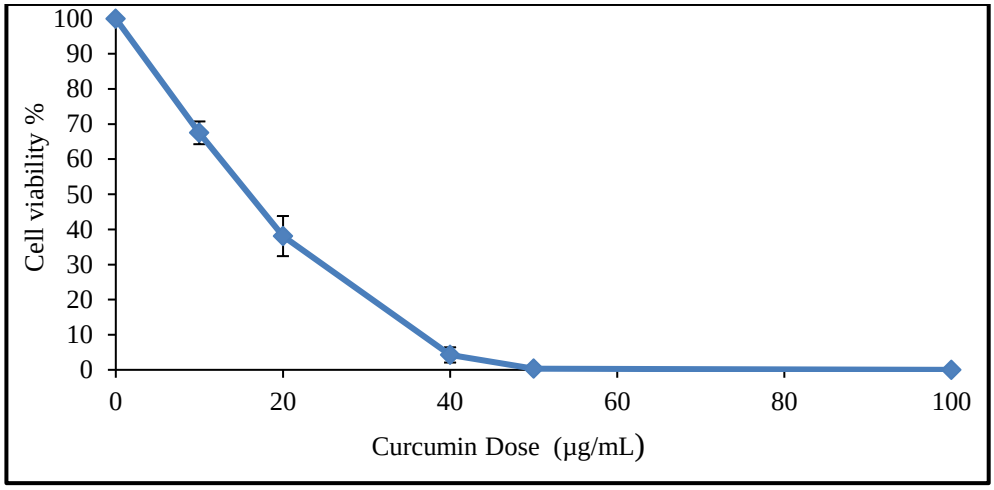

Fig. 4: Antiproliferative effects of pure CRC (curcumin) on LNCaP cells by means of MTT assay after 24 h incubation time. (n = 3).

The LNCaP cell lines viability was reduced to almost 0% at a very low drug concentration of 40 µg/mL. Several studies have demonstrated the efficiency of CRC as chemotherapeutic agent by presenting healing selectivity or superior killing of cancer cells without any substantial effects on normal cells [40-41]. According to Yang *et al.*, (2006), CRC could decrease the cellular proliferation and stimulate apoptosis in LNCaP cells in a concentration dependent manner [39]. The cytotoxicity of blank conjugated and unconjugated nanodispersions was evaluated to assess any significant changes in cell viability. As shown in Fig. 5, in a dose dependent study, both blank SLNs and Tf-SLNs showed negligible effects on cell viability with 91.7% and 90% respectively at concentrations of 1.5 mg/mL.

The reason for selecting CRC for the current study was due to the fact that previous studies has demonstrated its therapeutic potential for prostate cancer. CRC has been found to inhibit proliferation and angiogenesis while induces apoptosis to LNCaP cells line in *in vivo* studies [40]. In addition, transferrin was selected for active targeting of LNCaP cells as previous studies have demonstrated increased uptake and endocytosis in prostate cancer cells within the first 30 min [41].

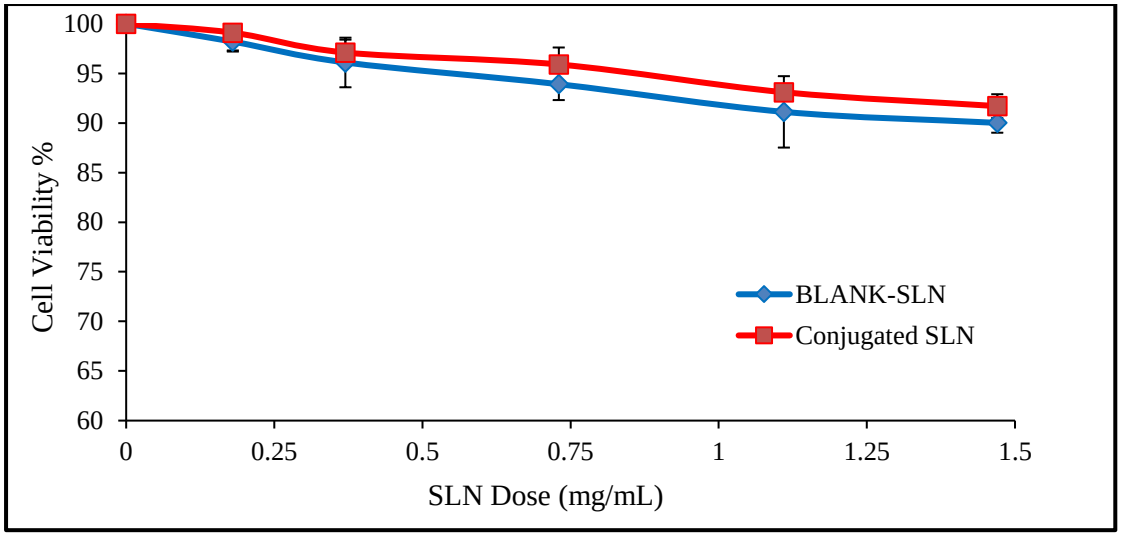

Fig. 5: Cytotoxicity of blank SLN formulations (blank and conjugated SLNs). (n = 3).

In case of CRC-SLN and Tf-CRC-SLN nanoparticles, cytotoxicity studies revealed enhanced antiproliferative activity in a dose dependant manner (Fig. 6). At the lowest CRC dose of 12.5 µg/mL the CRC-SLN and Tf-CRC-SLN dispersions presented substantial antiproliferative activity at 90.56% and 75.96% respectively.

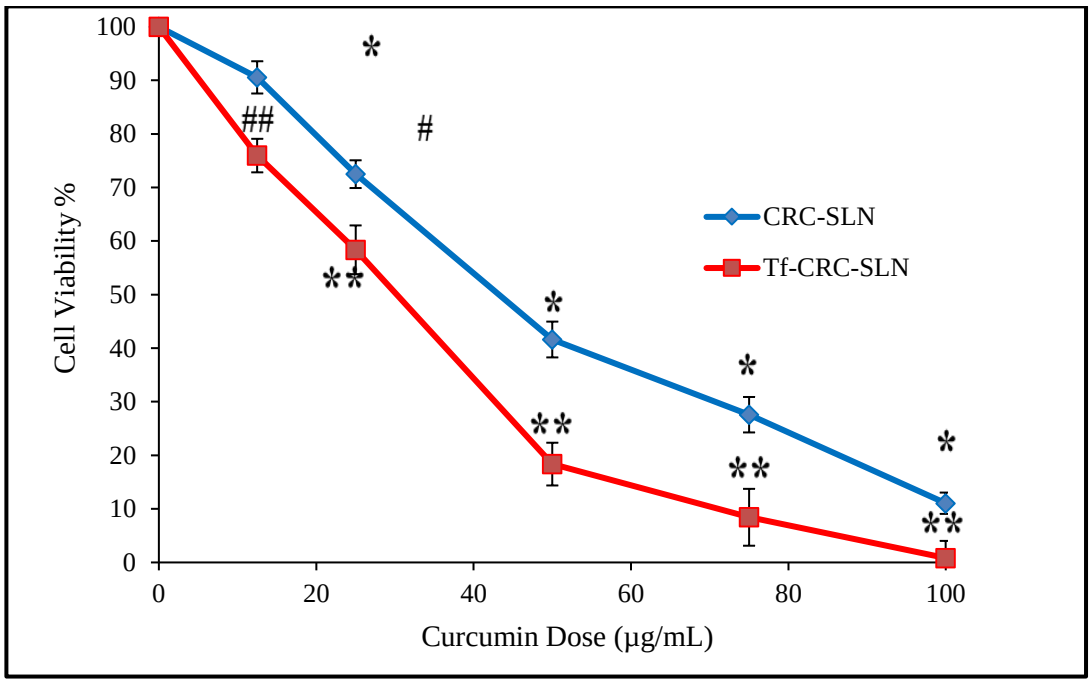

Fig. 6: Cytotoxicity of CRC-SLN and Tf-CRC-SLN after 24 h. Data is represented as mean ± S.D. (n = 3). #p=0.0366, *p< 0.0001, CRC-SLN (24 h) vs. blank SLN and ##p=0.0001, **p< 0.0001, Tf-CRC-SLN (48 h) vs. transferrin conjugated blank SLN.

The anticancer potency of Tf-CRC-SLN was significantly higher (14.6% more) than CRC-SLN nanoparticles. At increasing CRC concentrations of 50 µg/mL, both CRC-SLN and Tf-CRC-SLN decreased cell viability to 41.62% and 18.36% respectively. Consequently, 100 µg/mL CRC dose showed yet more pronounced effect where cell viability was decreased to 11.05% for CRC-SLN and 0.0% for the Tf-CRC-SLN nano-dispersions($p>0.01$). It can also be observed from Fig. 6 that Tf-CRC-SLNs nanoparticles exhibited a far more effective anti-proliferative activity compared to unconjugated SLNs suggesting successful active targeting which potentially could enhance the therapeutic potential of CRC. The cell viability of Tf-CRC-SLNs was further reduced to 0% after 48 h incubation (using CRC concentrations as before, data not presented) compared to the results obtained at 24 h due to further CRC release from the SLNs. According to Lemiux *et al*., (1994) transferrin can effectively inhibit p-glycoprotein efflux, raise cellular uptake and retention, which in turn results in an enhanced antiproliferative effect [42].

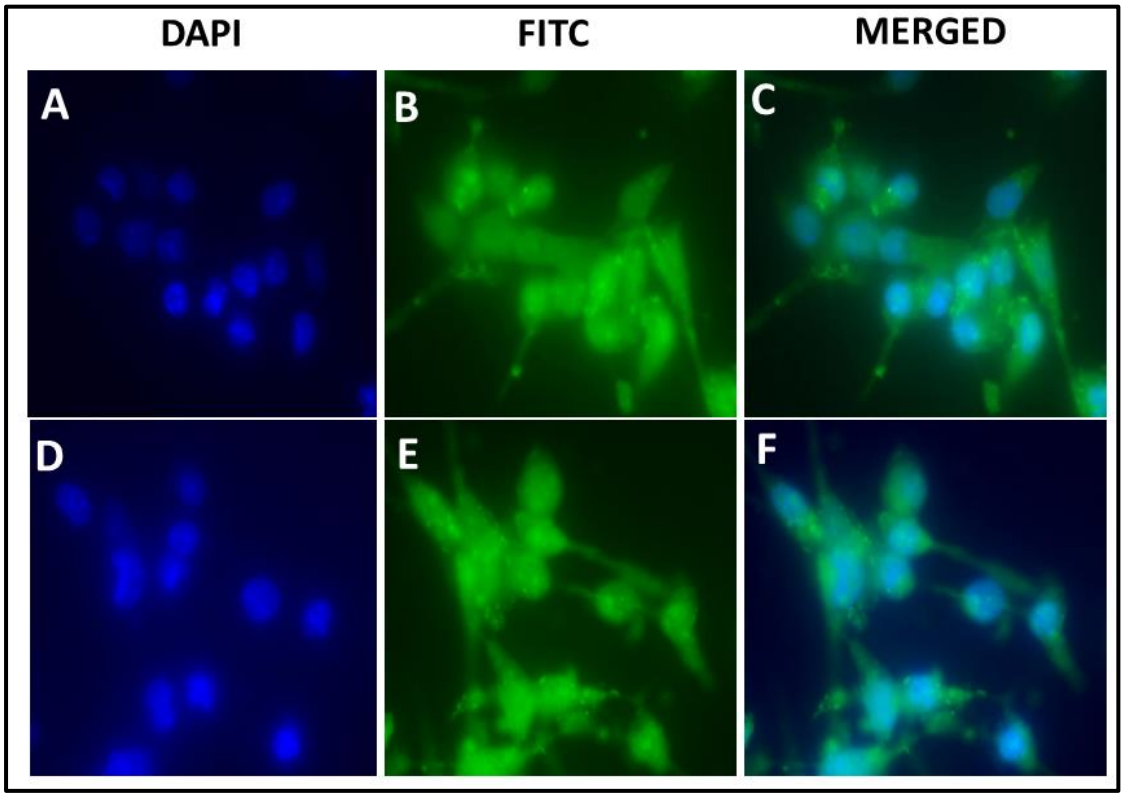

Fig. 7: Cellular uptake curcumin loaded SLNs. Green colour from FITC represents CRC. Blue colour from DAPI represents nuclei visualization. (A-C) shows the cellular uptake of Tf-CRC-SLN and (D-F) the uptake of CRC-SLN (50 µg/mL CRC).

3.4. Cellular uptake analysis using fluorescence microscopy

The internalization of SLN dispersions was confirmed by fluorescent microscopy where CRC-SLN and Tf-CRC-SLN were incubated in LNCaP prostate cancer cell line for 24 hours. Fig. 7 illustrates the cellular internalization of both CRC-SLN and Tf-CRC-SLN formulations in LNCaP prostate cancers cells where it be seen that the SLN particles are localised around the nucleus of the cytoplasm. Interestingly both CRC loaded SLNs (conjugated and unconjugated) showed similar uptake properties. The fluorescent intensity of encapsulated CRC was reduced due to the Tf conjugation on the surface of CRC-SLN. Several studies have proposed that SLNs are uptaken by the cells via the endocytosis mechanism pathway [43].

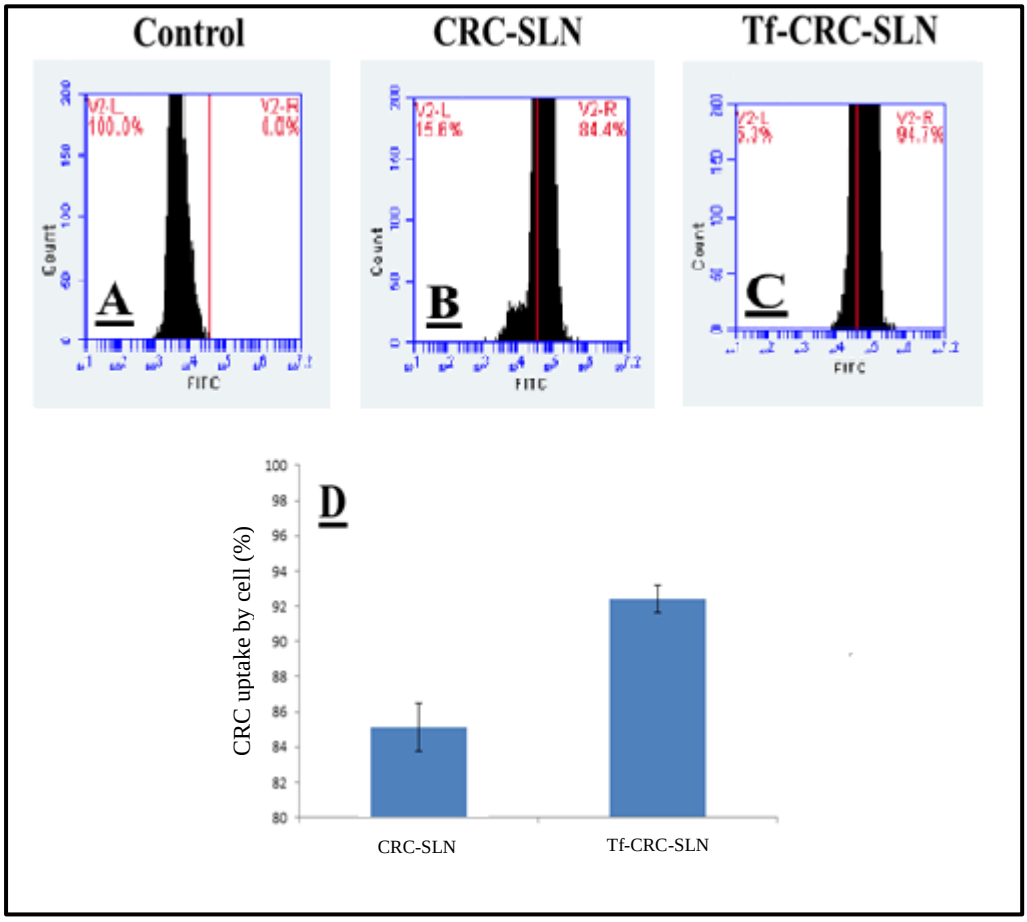

Fig. 8: Cell uptake of SLNs using FACS. (A) Cell uptake of control (Blank SLN). (B) Cellular uptake of CRC- SLN. (C) Cellular uptake of Tf-CRC- SLN. (D) Bar graphs representing the uptake of CRC-SLN and Tf-CRC-SLN (n = 3).

3.5. Flow cytometry analysis for cellular uptake of SLNs

Cellular uptake of CRC-SLN and Tf-CRC-SLN was examined quantitatively by using the intrinsic fluorescent property of CRC with fluorescent activated cell sorting (FACS)

analysis. CRC accumulated on LNCaP prostate cancer cell lines after 24 h incubation with both CRC-SLN and Tf-CRC-SLN (Fig. 8 B and C). Interestingly, a significantly higher percentage of cells (94.7±3 %) were identified as CRC positive when treated with Tf-CRC-SLN when compared with CRC-SLN treatment (80±2%, p=0.0146). The increase of fluorescent cell population containing CRC supports the usage of bioconjugated SLNs for targeted drug delivery system in prostate cancer [35].

3.6. *In-vitro* apoptosis study

The induction of apoptosis following treatment with CRC-SLN and Tf-CRC-SLN was measured using flow cytometry analysis (Fig. 9). Double staining allowed differentiation between live cells (Annex V negative, 7AAD negative) early apoptotic (Annex V positive, 7AAD negative) and necrotic or late apoptotic (PE Annexin V and 7AAD positive). Following treatment with pure CRC (15 µg/mL), 12±2.7% cells showed early apoptosis and 24±1.8% cells showed late apoptotic/necrotic features (Fig. 9).

The fraction of apoptotic cells varied along with the CRC loaded SLNs in a dose-correlated manner. Formulations with drug loading of 25 µg/mL did not show any significant variation among the early or late apoptotic cell population against the blank SLNs. However, 50 µg/mL Tf-CRC-SLN treated cells showed 19.9±4.1% early apoptotic and 55.1±4.9% late apoptotic/early necrotic cells populations, compared to 50 µg/mL CRC-SLN appeared with 24.5±4.8% early apoptotic and 34.0% late apoptotic/early necrotic cells populations for 24 h. Statistical analysis showed that 50 µg/mL Tf-CRC-SLN exhibited significant increase in late apoptotic/early necrotic cell population only ($p<0.05$) compared to the CRC loaded SLNs.

Treatment at 100 µg/mL induced a further increment of early apoptotic, late apoptotic and early necrotic cells populations. Cells incubated with CRC-SLN and Tf-CRC-SLN at 100 µg/mL dose exhibited with early apoptotic 12.1±2.6% and 6.4±1.1% respectively as well as late apoptotic/early necrotic populations of 80.3±2.1% and 88.9±1.3% respectively. In conclusion, an increased CRC dose resulted in a substantial increment ($p<0.01$) of late apoptotic/early necrotic cell population related to blank SLN's. The above results indicate that the CRC-SLN's surface modification with Tf improved the apoptotic activity in LNCaP cell line.

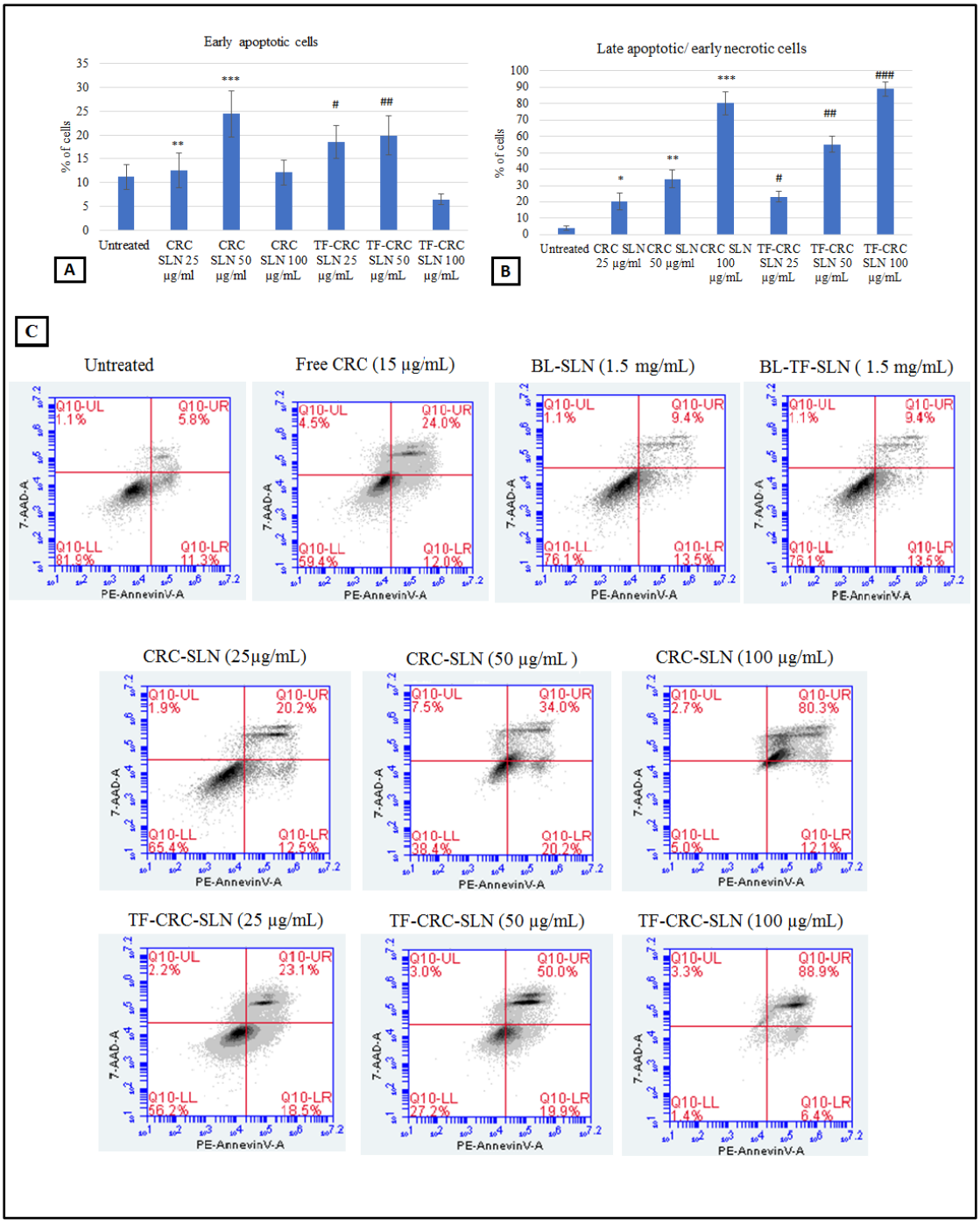

Fig. 9: Quantitative apoptotic determination in LNCaP cells with Blank SLN, Conjugated SLN, free CRC, CRC-SLN and Tf-CRC-SLN (A) Dose dependency on early apoptosis using concentrations of 25, 50 and 100 µg/mL of CRC-SLN and Tf-CRC-SLN dose for 24 h determined by FACS. (B) Dose dependency on late apoptosis using concentrations of 25, 50

and 100 µg/mL of CRC-SLN and Tf-CRC-SLN dose for 24 h. The findings are presented as bar chart (± S.D., n = 3). (*) $p<0.05$, Control versus CRC-SLN(25 µg/mL) and (#) $p<0.05$ Control versus vs Tf-CRC-SLN (25 µg/mL), (**) $p < 0.05$, Control vs. CRC-SLN and (##) $p<0.05$ Control vs. Tf-CRC-SLN (50 µg/mL), (***) $p< 0.05$, Control vs. CRC-SLN and (###) $p<0.05$ Control vs. Tf-CRC-SLN (100 µg/mL)(B) Dose dependency is presented as dot scheme of PE Annexin V versus 7-AAD. The dot representation from FACS shows the cell populations with necrotic cells at the top left, early apoptotic cells at the bottom left, late apoptotic cells/early necrotic cells at the top right and live cells in the bottom left end.

Similar findings have been previously reported where the conjugation of transferrin on the SLNs surface facilitated inhibition efficiency of the formulation [35,44,45]. Use of such a targeted drug delivery system can potentially minimise the highly necrotic behaviour of anticancer molecules, preventing unnecessary inflammation into the healthy cell compartments and lessen the side effects in patients during treatments [46].

3.7. *In-vivo* anti-tumour activity of bio-conjugated SLNs

In order to examine whether SLNs can enhance the *in-vivo* therapeutic efficiency of CRC by selectively targeting tumours, we treated BALB/c nude mice bearing LNCaP tumours. Indeed, during the 30 days treatment, the administration of both CRC-SLN and Tf-SLNs led to a marked tumour regression and to animal survival. The tumour inhibition growth in terms of mean tumour tissue weight is presented in Fig. 10. The examined therapeutic outcomes obtained by estimating the suppression of tumour growth in weight verified that SLN nanodispersions have better therapeutic efficacy compared to the pure drug solution.

Fig. 10 shows that CRC suppressed the total tumour tissue mass by 19%, n compared to the control at the completion of the treatment. Statistical analysis of an unpaired t-test revealed that, the effect of CRC on total tumour tissue weight upon treatment was considerably higher than the control ($p<0.02$). Blank SLNs did not show any tumour regression when compared with the control samples. Further improvement was observed for unconjugated CRC-SLNs showing tumour regression at 52% compared to CRC ethanolic solutions. Significant difference can be observed in the therapeutic efficiency between blank SLN and CRC-SLN formulations ($p<0.0001$) where the

inhibition of the tumour growth mass reached 61% compared to blank SLN formulations.

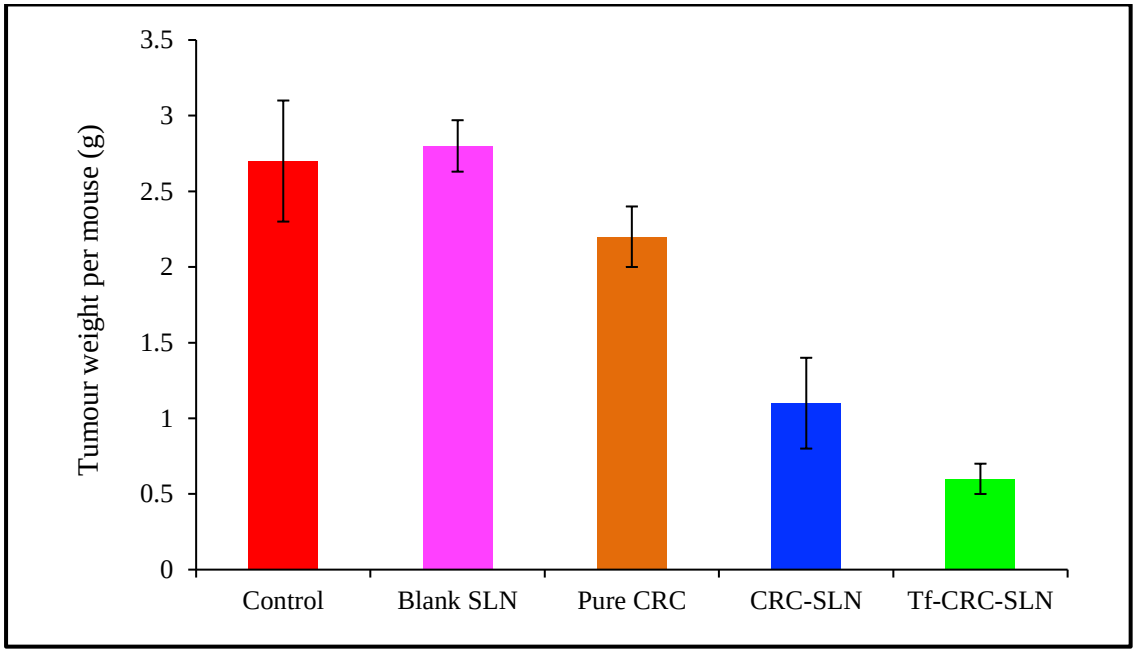

Fig. 10: Comparative therapeutic effects of control, blank SLN, pure CRC, CRC-SLN and Tf-CRC-SLN on tumour suppression of LNCaP prostate cancer.

The comparison of CRC and CRC-SLN demonstrated a significantly higher antitumor activity for the latter and the tumour mass was reduced to an additional 42%, compared to the CRC ethanol solution. Fig. 10 also depicts the therapeutic efficacy of Tf-CRC-SLN where at the end of the treatment functionalized SLNs demonstrated a profound effect in the suppression of tumour growth by 79% and greater survival rate to the mice administered CRC-SLN and CRC ethanol solutions. This resulted in a significant improvement of therapeutic efficiency of CRC for the healing of tumours as previously described by Fu *et al.*, 2011 [47]. The tumour regression observed for Tf-CRC-SLN might result from several factors. Firstly, the entrapment of CRC within the lipid matrix of the SLN offers the opportunity to administer the drug intravenously while at the same time protecting it from degradation and metabolism due to the solid lipid core [48]. In turn this ensured sufficient CRC circulation for reaching the tumours [47]. Moreover, a higher dose of CRC can be administered as an outcome of the increased drug encapsulation in SLNs which resulted in the dosing treatment and therapeutic index optimization. The increase of treatment period has also played a significant role in the obtained improvement. Furthermore, Tf-conjugated CRC-SLN nanoparticles might have diverse intracellular pathways after uptake through transferring receptor

facilitated endocytosis in comparison to unconjugated SLNs *by* a non-specific route which in turn alters the intracellular retention and thus, therapeutic efficiency of the loaded CRC [35]. The tumour weight regression of the various groups was reduced in the following ascending order: CRC (19%) < CRC-SLN (61%) < Tf-CRC-SLN (79%). The therapeutic effect was also investigated by quantifying the suppression of tumour growth specified in terms of tumour volume confirms that both CRC and CRC encapsulated SLN formulations can inhibit tumour growth (Fig. 11). As a result, CRC treatment produced higher tumour inhibition when compared with control (Fig. 11). After treatment for 30 days with CRC solution, the observed tumour volume was 1153.13 mm^3, while at the same time control exhibited a tumour volume of 1410.21 mm^3.

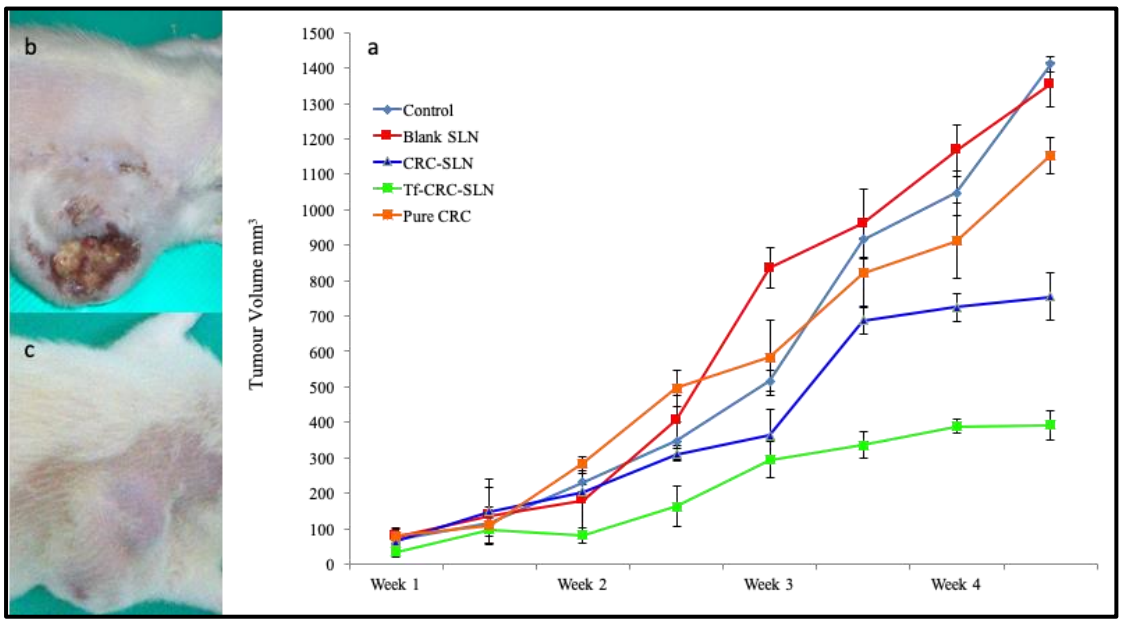

Fig. 11: a) Therapeutic effect of control, blank SLN, pure CRC, CRC-SLN and Tf-CRC-SLN on mice bearing tumour, b) control mice (week 4) and c) Tf – CRC – SLN treated mice (week 4).

Statistical analysis using t-test shows that CRC effect on tumour growth regression is significantly different from the control treatment ($P < 0.0001$). These findings can confirm that, CRC can induce an effective therapeutic effect on the LNCaP prostate cancer tumours. Fig. 11 also shows that blank SLN formulation did not have any effect in tumour growth suppression, similarly to the control treatment ($P = 0.09$). However, CRC-SLN and Tf-CRC-SLN exhibited significant decrease in tumour growth when

comparing to CRC solution treatment, blank SLN and the control. Tf-CRC-SLN presented the highest tumour growth inhibition up to 72% when compared to the control. The observed tumour volume of mice treated with Tf-CRC-SLN was 392.64 mm^3 compared to CRC-SLN (754.59 mm^3), CRC (1153.13 mm^3), blank SLN (1354.08) and control 1410.21 mm^3).

A summary graph of tumour regression efficiency of CRC and CRC – SLN formulations is shown in Fig. 12. Statistical analysis using ANOVA shows that difference of therapeutic efficacy between the treatments administered in tumour bearing mice is highly significant. Finally, as shown in Fig. 13 the treatment waw well endured by the animals and no evident toxicity or weight reduction was detected.

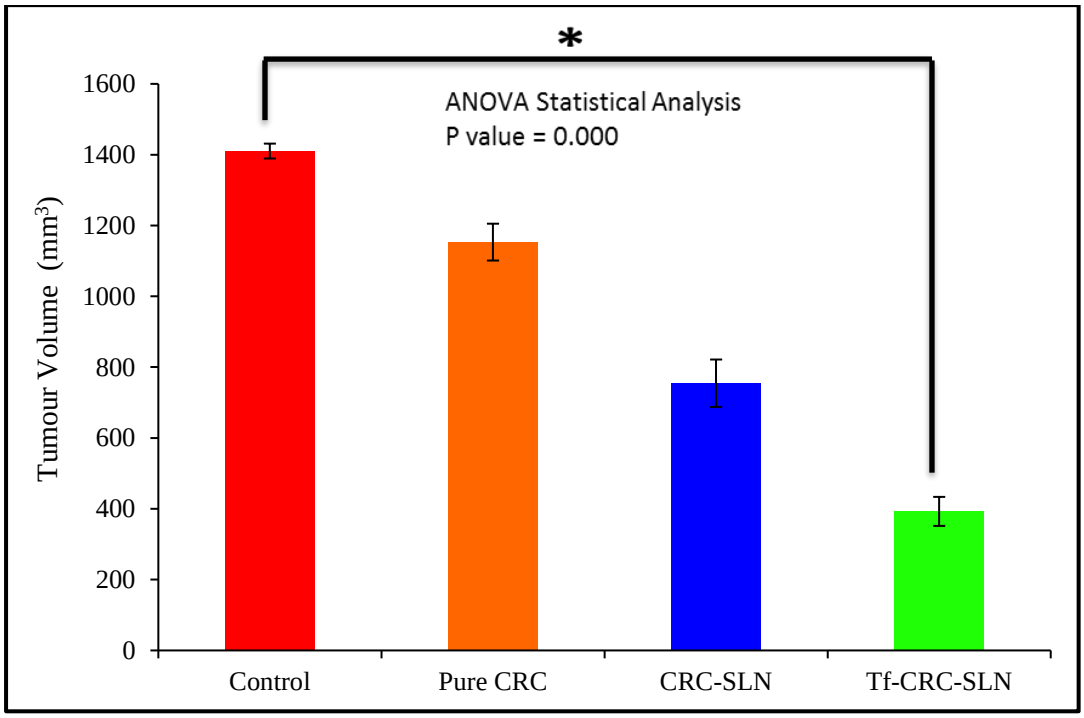

Fig. 12: Difference in therapeutic efficiency of control, pure CRC, CRC-SLN and Tf-CRC-SLN formulations in mice bearing tumour.

CRC is a main component of turmeric and it has been proved highly effective, in animal trials, for tumour cure stimulated by a number of chemical carcinogens [49]. CRC also exerts strong antioxidant and anti-inflammatory action through the suppression of the nuclear factor- ƙB (NF-ƙB) and the activation of activator protein-1 [50]. Despite of the above features CRC bioavailability limits its therapeutic efficiency. As demonstrated from these *in-vivo* trials, drug loaded SLN and Tf-SLNs suppressed the tumour volume

significantly when compared to the bulk drug; comparable findings were also reported by Chen *et al*., (2012) [51].

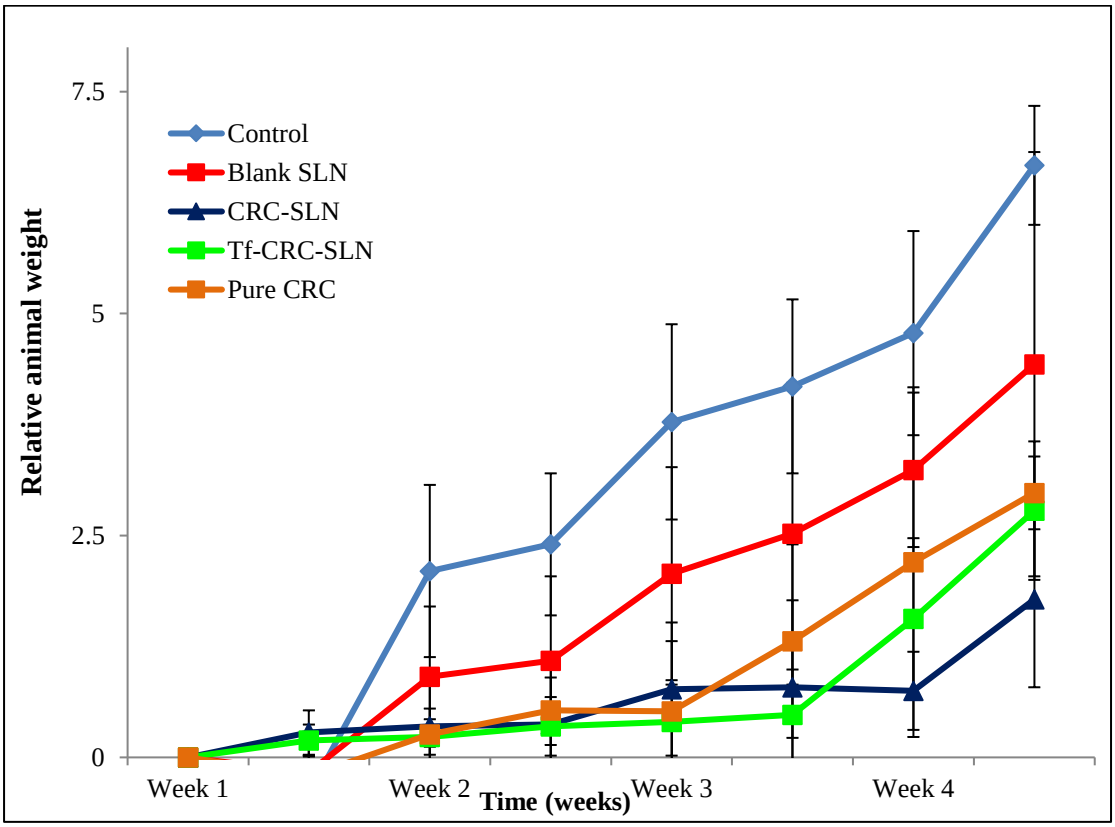

Fig. 13: Treatment tolerance by mice bearing tumour over the treatment study period of four weeks.

4. Conclusions

In conclusion, we have demonstrated that bioconjugated Tf- SLNs loaded with CRC can induce significant tumour suppression in mice bearing prostate cancer. The CRC encapsulation in bioconjugated SLNs improved the drug uptake when compared to drug-ethanol solution and unconjugated SLNs. In addition, Tf-SLNs were proved as an excellent CRC carrier by preventing drug degradation while the nano-dispersions were also stable during long-term storage. Therefore, results presented in this study suggest that Tf-SLNs can potentially act as an actively targeted drug carrier and worth further exploitation for the treatment of prostate cancer.

Conflict of interest

There are no conflicts of interest to declare

References

[1] G.Y. Melmed, L. Kwan, K. Reid, M.S. Litwin, Quality of life at the end of life: trends in patients with metastatic prostate cancer, Urology. 59 (2002) 103–109.

[2] R. Siegel, C. DeSantis, K. Virgo, K. Stein, A. Mariotto, T. Smith, D. Cooper, T. Gansler, C. Lerro, S. Fedewa, Cancer treatment and survivorship statistics, 2012, CA. Cancer J. Clin. 62 (2012) 220–241.

[3] R. Siegel, D. Naishadham, A. Jemal, Cancer statistics for hispanics/latinos, 2012, CA. Cancer J. Clin. 62 (2012) 283–298.

[4] A. Caplan, A. Kratz, Prostate-specific antigen and the early diagnosis of prostate cancer, Pathol. Patterns Rev. 117 (2002) S104–S108.

[5] Y. Patil, H. Shmeeda, Y. Amitay, P. Ohana, S. Kumar, A. Gabizon, Targeting of folate-conjugated liposomes with co-entrapped drugs to prostate cancer cells via prostate-specific membrane antigen (PSMA), Nanomedicine Nanotechnology, Biol. Med. 14 (2018) 1407–1416. https://doi.org/https://doi.org/10.1016/j.nano.2018.04.011.

[6] K. Poudel, R.K. Thapa, M. Gautam, W. Ou, Z.C. Soe, B. Gupta, H.B. Ruttala, H.N. Thuy, P.C. Dai, J.-H. Jeong, S.K. Ku, H.-G. Choi, C.S. Yong, J.O. Kim, Multifaceted NIR-responsive polymer-peptide-enveloped drug-loaded copper sulfide nanoplatform for chemo-phototherapy against highly tumorigenic prostate cancer, Nanomedicine Nanotechnology, Biol. Med. 21 (2019) 102042. https://doi.org/https://doi.org/10.1016/j.nano.2019.102042.

[7] A.A. Shitole, N. Sharma, P. Giram, A. Khandwekar, M. Baruah, B. Garnaik, S. Koratkar, LHRH-conjugated, PEGylated, poly-lactide-co-glycolide nanocapsules for targeted delivery of combinational chemotherapeutic drugs Docetaxel and Quercetin for prostate cancer, Mater. Sci. Eng. C. 114 (2020) 111035. https://doi.org/https://doi.org/10.1016/j.msec.2020.111035.

[8] R. Stephenson, P. Varamini, N. Butcher, R. Minchin, I. Toth, Effect of lipidated gonadotropin-releasing hormone peptides on receptor mediated binding and uptake into prostate cancer cells in vitro, Nanomedicine Nanotechnology, Biol. Med. 10 (2014) 1799–1808. https://doi.org/https://doi.org/10.1016/j.nano.2014.06.015.

[9] P.-Y. Chu, S.-C. Tsai, H.-Y. Ko, C.-C. Wu, Y.-H. Lin, Co-delivery of natural compounds with a dual-targeted nanoparticle delivery system for improving synergistic therapy in an orthotopic tumor model, ACS Appl. Mater. Interfaces. 11 (2019) 23880–23892.

[10] H. Tan, N. Hou, Y. Liu, B. Liu, W. Cao, D. Zheng, W. Li, Y. Liu, B. Xu, Z. Wang, D. Cui, CD133 antibody targeted delivery of gold nanostars loading IR820 and docetaxel for multimodal imaging and near-infrared photodynamic/photothermal/chemotherapy against castration resistant prostate cancer, Nanomedicine Nanotechnology, Biol. Med. 27 (2020) 102192. https://doi.org/https://doi.org/10.1016/j.nano.2020.102192.

[11] R.H. Perera, A. de Leon, X. Wang, Y. Wang, G. Ramamurthy, P. Peiris, E.

Abenojar, J.P. Basilion, A.A. Exner, Real time ultrasound molecular imaging of prostate cancer with PSMA-targeted nanobubbles, Nanomedicine Nanotechnology, Biol. Med. 28 (2020) 102213. https://doi.org/https://doi.org/10.1016/j.nano.2020.102213.

[12] T. Yin, K. Wang, C. Qiu, X. Zhang, H. Zhou, Y. You, J. Ren, R. Mao, B. Yang, X. Miao, J. Tian, R. Zheng, Simple structural indocyanine green-loaded microbubbles for dual-modality imaging and multi-synergistic photothermal therapy in prostate cancer, Nanomedicine Nanotechnology, Biol. Med. 28 (2020) 102229. https://doi.org/https://doi.org/10.1016/j.nano.2020.102229.

[13] R.K. Thapa, H.T. Nguyen, J.-H. Jeong, B.S. Shin, S.K. Ku, H.-G. Choi, C.S. Yong, J.O. Kim, Synergistic anticancer activity of combined histone deacetylase and proteasomal inhibitor-loaded zein nanoparticles in metastatic prostate cancers, Nanomedicine Nanotechnology, Biol. Med. 13 (2017) 885–896. https://doi.org/https://doi.org/10.1016/j.nano.2016.12.010.

[14] J.C. Evans, M. Malhotra, J. Guo, J.P. O'Shea, K. Hanrahan, A. O'Neill, W.D. Landry, B.T. Griffin, R. Darcy, R.W. Watson, C.M. O'Driscoll, Folate-targeted amphiphilic cyclodextrin.siRNA nanoparticles for prostate cancer therapy exhibit PSMA mediated uptake, therapeutic gene silencing in vitro and prolonged circulation in vivo, Nanomedicine Nanotechnology, Biol. Med. 12 (2016) 2341–2351. https://doi.org/https://doi.org/10.1016/j.nano.2016.06.014.

[15] D.J. Bharali, T. Sudha, H. Cui, B.M. Mian, S.A. Mousa, Anti-CD24 nano-targeted delivery of docetaxel for the treatment of prostate cancer, Nanomedicine Nanotechnology, Biol. Med. 13 (2017) 263–273. https://doi.org/https://doi.org/10.1016/j.nano.2016.08.017.

[16] J. Sun, C. Bi, H.M. Chan, S. Sun, Q. Zhang, Y. Zheng, Curcumin-loaded solid lipid nanoparticles have prolonged in vitro antitumour activity, cellular uptake and improved in vivo bioavailability, Colloids Surfaces b Biointerfaces. 111 (2013) 367–375.

[17] D. Pozzi, V. Colapicchioni, G. Caracciolo, S. Piovesana, A.L. Capriotti, S. Palchetti, S. De Grossi, A. Riccioli, H. Amenitsch, A. Laganà, Effect of polyethyleneglycol (PEG) chain length on the bio–nano-interactions between PEGylated lipid nanoparticles and biological fluids: from nanostructure to uptake in cancer cells, Nanoscale. 6 (2014) 2782–2792.

[18] R. Paliwal, S. Rai, B. Vaidya, K. Khatri, A.K. Goyal, N. Mishra, A. Mehta, S.P. Vyas, Effect of lipid core material on characteristics of solid lipid nanoparticles designed for oral lymphatic delivery, Nanomedicine Nanotechnology, Biol. Med. 5 (2009) 184–191.

[19] Y.-P. Fang, P.-C. Wu, Y.-B. Huang, C.-C. Tzeng, Y.-L. Chen, Y.-H. Hung, M.-J. Tsai, Y.-H. Tsai, Modification of polyethylene glycol onto solid lipid nanoparticles encapsulating a novel chemotherapeutic agent (PK-L4) to enhance solubility for injection delivery, Int. J. Nanomedicine. 7 (2012) 4995.

[20] C.-H. Chuang, P.-C. Wu, T.-H. Tsai, Y.-P. Fang, Y.-H. Tsai, T.-C. Cheng, C.-C. Huang, M.-Y. Huang, F.-M. Chen, Y.-C. Hsieh, Development of pH-sensitive cationic PEGylated solid lipid nanoparticles for selective cancer-targeted

therapy, J. Biomed. Nanotechnol. 13 (2017) 192–203.

[21] Y. Kuang, K. Zhang, Y. Cao, X. Chen, K. Wang, M. Liu, R. Pei, Hydrophobic IR-780 dye encapsulated in cRGD-conjugated solid lipid nanoparticles for NIR imaging-guided photothermal therapy, ACS Appl. Mater. Interfaces. 9 (2017) 12217–12226.

[22] R. Karim, E. Lepeltier, L. Esnault, P. Pigeon, L. Lemaire, C. Lépinoux-Chambaud, N. Clere, G. Jaouen, J. Eyer, G. Piel, Enhanced and preferential internalization of lipid nanocapsules into human glioblastoma cells: effect of a surface-functionalizing NFL peptide, Nanoscale. 10 (2018) 13485–13501.

[23] A. Widera, F. Norouziyan, W.-C. Shen, Mechanisms of TfR-mediated transcytosis and sorting in epithelial cells and applications toward drug delivery, Adv. Drug Deliv. Rev. 55 (2003) 1439–1466.

[24] S.K. Sahoo, V. Labhasetwar, Enhanced antiproliferative activity of transferrin-conjugated paclitaxel-loaded nanoparticles is mediated via sustained intracellular drug retention, Mol. Pharm. 2 (2005) 373–383.

[25] K. Maruyama, O. Ishida, S. Kasaoka, T. Takizawa, N. Utoguchi, A. Shinohara, M. Chiba, H. Kobayashi, M. Eriguchi, H. Yanagie, Intracellular targeting of sodium mercaptoundecahydrododecaborate (BSH) to solid tumors by transferrin-PEG liposomes, for boron neutron-capture therapy (BNCT), J. Control. Release. 98 (2004) 195–207.

[26] J.-L. Li, L. Wang, X.-Y. Liu, Z.-P. Zhang, H.-C. Guo, W.-M. Liu, S.-H. Tang, In vitro cancer cell imaging and therapy using transferrin-conjugated gold nanoparticles, Cancer Lett. 274 (2009) 319–326.

[27] K. Ulbrich, T. Hekmatara, E. Herbert, J. Kreuter, Transferrin-and transferrin-receptor-antibody-modified nanoparticles enable drug delivery across the blood–brain barrier (BBB), Eur. J. Pharm. Biopharm. 71 (2009) 251–256.

[28] S.G. Potta, S. Minemi, R.K. Nukala, C. Peinado, D.A. Lamprou, A. Urquhart, D. Douroumis, Preparation and characterization of ibuprofen solid lipid nanoparticles with enhanced solubility, J. Microencapsul. 28 (2011) 74–81.

[29] X. Li, L. Ding, Y. Xu, Y. Wang, Q. Ping, Targeted delivery of doxorubicin using stealth liposomes modified with transferrin, Int. J. Pharm. 373 (2009) 116–123.

[30] A. Yousefi, F. Esmaeili, S. Rahimian, F. Atyabi, R. Dinarvand, Preparation and in vitro evaluation of a pegylated nano-liposomal formulation containing docetaxel, Sci. Pharm. 77 (2009) 453–464.

[31] C. Freitas, R.H. Müller, Effect of light and temperature on zeta potential and physical stability in solid lipid nanoparticle (SLN^{TM}) dispersions, Int. J. Pharm. 168 (1998) 221–229.

[32] C. Schwarz, W. Mehnert, J.S. Lucks, R.H. Müller, Solid lipid nanoparticles (SLN) for controlled drug delivery. I. Production, characterization and sterilization, J. Control. Release. 30 (1994) 83–96.

[33] H. Ali, A.B. Shirode, P.W. Sylvester, S. Nazzal, Preparation, characterization,

and anticancer effects of simvastatin–tocotrienol lipid nanoparticles, Int. J. Pharm. 389 (2010) 223–231.

[34] G.T. Hermanson, Bioconjugate techniques, Academic press, 2013.

[35] R.S. Mulik, J. Mönkkönen, R.O. Juvonen, K.R. Mahadik, A.R. Paradkar, Transferrin mediated solid lipid nanoparticles containing curcumin: Enhanced in vitro anticancer activity by induction of apoptosis, Int. J. Pharm. 398 (2010) 190–203. https://doi.org/10.1016/j.ijpharm.2010.07.021.

[36] W. Tiyaboonchai, W. Tungpradit, P. Plianbangchang, Formulation and characterization of curcuminoids loaded solid lipid nanoparticles, Int. J. Pharm. 337 (2007) 299–306.

[37] Z. Liu, P. Huang, S. Law, H. Tian, W. Leung, Preventive Effect of Curcumin Against Chemotherapy-Induced, 9 (2018) 1–9. https://doi.org/10.3389/fphar.2018.01374.

[38] B.L. Tan, Curcumin Combination Chemotherapy : The Implication and E ffi cacy in Cancer, 2 (2019) 1–21.

[39] L. Yang, L. Chen, B. Meng, J. Suo, H. Wang, H. Xie, Q. Jin, L. Yao, R. Wang, L. Zhang, The effect of curcumin on proliferation and apoptosis in LNCaP prostate cancer cells, Chinese J. Clin. Oncol. 3 (2006) 55–60.

[40] T. Dorai, Y. Cao, B. Dorai, R. Buttyan, A.E. Katz, Therapeutic potential of curcumin in human prostate cancer. III. Curcumin inhibits proliferation, induces apoptosis, and inhibits angiogenesis of LNCaP prostate cancer cells in vivo, Prostate. 47 (2001) 293–303.

[41] I.R.D. Johnson, E.J. Parkinson-Lawrence, T. Shandala, R. Weigert, L.M. Butler, D.A. Brooks, Altered endosome biogenesis in prostate cancer has biomarker potential, Mol. Cancer Res. 12 (2014) 1851–1862.

[42] P. Lemieux, M. Page, Sensitivity of multidrug-resistant MCF-7 cells to a transferrin-doxorubicin conjugate., Anticancer Res. 14 (1994) 397–403.

[43] C. Mohanty, S.K. Sahoo, The in vitro stability and in vivo pharmacokinetics of curcumin prepared as an aqueous nanoparticulate formulation, Biomaterials. 31 (2010) 6597–6611.

[44] Y. Gupta, A. Jain, S.K. Jain, Transferrin-conjugated solid lipid nanoparticles for enhanced delivery of quinine dihydrochloride to the brain, J. Pharm. Pharmacol. 59 (2007) 935–940.

[45] R.S. Mulik, J. Mönkkönen, R.O. Juvonen, K.R. Mahadik, A.R. Paradkar, Apoptosis-induced anticancer effect of transferrin-conjugated solid lipid nanoparticles of curcumin, Cancer Nanotechnol. 3 (2012) 65–81. https://doi.org/10.1007/s12645-012-0031-2.

[46] Z. Liu, P. Huang, S. Law, H. Tian, W. Leung, C. Xu, Preventive effect of curcumin against chemotherapy-induced side-effects, Front. Pharmacol. 9 (2018) 1374.

[47] J.Y. Fu, W. Zhang, D.R. Blatchford, L. Tetley, G. McConnell, C. Dufès, Novel tocotrienol-entrapping vesicles can eradicate solid tumors after intravenous administration, J. Control. Release. 154 (2011) 20–26.

[48] H. Bunjes, M. Drechsler, M.H.J. Koch, K. Westesen, Incorporation of the model drug ubidecarenone into solid lipid nanoparticles, Pharm. Res. 18 (2001) 287–293.

[49] M.-T. Huang, R.C. Smart, C.-Q. Wong, A.H. Conney, Inhibitory effect of curcumin, chlorogenic acid, caffeic acid, and ferulic acid on tumor promotion in mouse skin by 12-O-tetradecanoylphorbol-13-acetate, Cancer Res. 48 (1988) 5941–5946.

[50] T. Hour, J. Chen, C. Huang, J. Guan, S. Lu, Y. Pu, Curcumin enhances cytotoxicity of chemotherapeutic agents in prostate cancer cells by inducing p21WAF1/CIP1 and C/EBPβ expressions and suppressing NF-κB activation, Prostate. 51 (2002) 211–218.

[51] Y. Chen, Q. Wu, Z. Zhang, L. Yuan, X. Liu, L. Zhou, Preparation of curcumin-loaded liposomes and evaluation of their skin permeation and pharmacodynamics, Molecules. 17 (2012) 5972–5987.